Equilibria of Aqueous System Phases Containing Arsenic + Iron and Arsenic + Calcium at (323.15 and 343.15) K

María E. Taboada,* Pía C. Hernández, Elsa K. Flores, Héctor R. Galleguillos, and Teófilo A. Graber

Departamento de Ingeniería Química, Universidad de Antofagasta, CICITEM, Av. Angamos 601, Antofagasta, Chile

The present study includes solubility measurements, density, and refractive indices of saturated solutions of the systems $As_2O_5 + Fe(OH)_3 + H_2O$ and $As_2O_5 + CaCO_3 + H_2O$. The experimental study was carried out at (323.15 and 343.15) K and for different mass fractions of arsenic, iron, and calcium. With the experimental results obtained, phase diagrams at these two temperatures and their regions were determined. The most important precipitated salt for the first system was $FeAsO_4 \cdot 2H_2O$ (scorodite) and for the second system $CaHAsO_4 \cdot H_2O$ (haidingerite). The experimental data on solubility and physical properties as a function of the mass fraction of iron and calcium were correlated for both systems. These equations allowed determination of the invariant points (double saturation equilibrium) of both systems for the two temperatures studied in this work and verified by scanning electron microscopy by the second system. This work is a contribution to the mining industry, to fix arsenic to solid matrices from industrial liquid residues.

1. Introduction

Chile is the main copper producer of the world with 37.5 % of the world production, which represents an income of more than $18 billion, with 16 % of the total GDP of the country. One problem associated with this industry is arsenic contained in sulfide ores. These ores are readily concentrated by froth flotation and are treated in a variety of ways. Whichever method of treatment is used, arsenical waste remains that necessitates stabilization and storage over the long-term. This is a common problem with other copper producing countries, like Canada and Australia. In this work, the phase equilibria and conditions required to crystallize arsenic in stable solids have been studied, and in this regard, the equilibria of arsenic + iron and arsenic + calcium species in aqueous solution are important.

Arsenical wastes can be generated from other processes of metal production such as lead, zinc, gold, and silver. Arsenic is also released into the environment by the dispersion of arsenic-containing fertilizers, pesticides, and wood preservatives.[1,2]

Traditionally, the role of crystallization and phase equilibrium dynamics of mineral effluents were not considered important, but they have recently become more relevant due to increasing environmental awareness and more stringent regulations for the handling and disposal of arsenic compounds. Properties of waste products such as high chemical stability, compactness, and high density in a crystalline form can be obtained through crystallization-based treatment processes.

Crystalline ferric arsenate has been recommended as an alternative compound for the deposition of arsenic, because it is stable, is insoluble in water, and has a high arsenic concentration in its structure.

Ugarte[3] has explained that the Fe(III)−As(V) system has several solid phases, which tend to be amorphous at temperatures below 363.15 K because the arsenic ions are adsorbed in a ferric hydroxide gel. With an initial Fe/As molar ratio near 1 and temperatures above 423.15 K, a Type One ($Fe_2(HAsO_4)_3 \cdot xH_2O$) phase is formed. The solubility of the precipitate formed according to TCLP tests (Toxicity Characteristic Leaching Procedure) is > 5 $mg \cdot L^{-1}$ (as As). If the initial Fe/As molar ratio is bigger than or similar to 1.5 at temperatures between (423.15 and 473.15) K, a crystalline ferric arsenate, identical to the mineral scorodite, is formed. If the temperature is above 473.15 K, the ferric arseno-hydroxy-sulfate phase ($Fe_3(AsO_4)_2(SO_4)(OH)$), of Type Two, that has a solubility < 5 $mg \cdot L^{-1}$ (as As), is formed.

Swash and Monhemius[4] found that amorphous ferric arsenates have a higher solubility than that of crystalline scorodite by over 2 orders of magnitude. It was also observed that ferric arsenates begin to precipitate at pH values of between 1 and 2, while the formation of calcium arsenates begins at a pH of between 3 and 4.

Richmond et al.[5] studied the removal of the arsenate anion from aqueous solution by coprecipitation with ferrihydrite (iron oxide−hydroxide) because it easily fixes AsO_4^{3-}. The Fe/As molar ratio remained constant at 12, while the pH (3.5, 5.5, 7) and Fe concentration were varied. It was found that residual arsenic decreases at a low pH because the positive surface charge of the ferrihydrite increases, which indicates a great affinity of the arsenate anion with the surface of the ferrihydrite, and a higher quotient of the oversaturation is required to remove the same quantity of arsenic at pH 7 than is required at pH 3.5. In general, this study suggests that the absorption of arsenate on ferrihydrite is rapid and effective to remove arsenic by controlling pH and oversaturation.

Demopoulos[6] obtained scorodite at ambient pressure and a temperature of 368.15 K, from sulfate containing effluents, using H_2SO_4, 1 $g \cdot L^{-1}$ of As(V), and a Fe/As molar ratio equal to 1. In this study, a strict control of pH was made, neutralizing with NaOH for 4 h at pH = 2. When the pH is 0.5, 4 $g \cdot L^{-1}$ of seed was added. Crystallization of scorodite was obtained when the pH reached a value of 1.5, which is equivalent to pH from induction. This pH is defined as the pH at which the onset of homogeneous nucleation is observed. The yield was only 65 %. On the other hand, lime (CaO) is very commonly used for treating an industrial byproduct with arsenic.

* Corresponding author. Phone: 56-55-637313. E-mail: mtaboada@uantof.cl.

10.1021/je900151s CCC: $40.75
Published on Web 07/07/2009

Table 1. Solubility w (Mass Fraction) of As(1) and Fe(2), Refractive Index, n_D, and Density, ρ, for the $As_2O_5 + Fe(OH)_3 + H_2O$ System at 323.15 K

w_1	w_2	solid phase	n_D	ρ (g·cm^{-3})
0.0000	0.0000	$FeSO_4(OH)(H_2O)_2$	1.3298	0.99205
0.0023	0.0000	$FeSO_4(OH)(H_2O)_2$	1.3389	1.04892
0.0060[a]	**0.0002**	**$FeSO_4(OH)(H_2O)_2$ + $FeAsO_4 \cdot 2H_2O$**	**1.3312**[a]	**0.99860**[a]
0.0257	0.0000	$FeAsO_4 \cdot 2H_2O$	1.3340	1.02510
0.0439	0.0001	$FeAsO_4 \cdot 2H_2O$	1.3371	1.07380
0.1036	0.0001	$FeAsO_4 \cdot 2H_2O$	1.3488	1.15610
0.1140	0.0002	$FeAsO_4 \cdot 2H_2O$	1.3620	1.21200
0.1632	0.0061	$FeAsO_4 \cdot 2H_2O$	1.3661	1.28150
0.1710[a]	**0.0086**	**$FeAsO_4 \cdot 2H_2O$ + $Fe(H_2AsO_4)_3 \cdot 5H_2O$**	**1.3748**[a]	**1.29089**[a]
0.1923	0.0060	$Fe(H_2AsO_4)_3 \cdot 5H_2O$	1.3799	1.34957
0.2555	0.0022	$Fe(H_2AsO_4)_3 \cdot 5H_2O$	1.3911	1.44750
0.2946	0.0018	$Fe(H_2AsO_4)_3 \cdot 5H_2O$	1.4127	1.64420
0.3843	0.0039	$Fe(H_2AsO_4)_3 \cdot 5H_2O$	1.4415	1.85310
0.4249	0.0042	$Fe(H_2AsO_4)_3 \cdot 5H_2O$	1.4580	1.96580
0.4790	0.0022	$Fe(H_2AsO_4)_3 \cdot 5H_2O$	1.4765	2.14970

[a] Data from curve fit to eqs 2 and 3.

Table 2. Solubility w (Mass Fraction) of As(1) and Fe(2), Refractive Index, n_D, and Density, ρ, for the $As_2O_5 + Fe(OH)_3 + H_2O$ System at 343.15 K

w_1	w_2	solid phase	n_D	ρ (g·cm^{-3})
0.0017	0.0000	$FeAsO_4 \cdot 2H_2O$	1.3279	0.99692
0.0106	0.0000	$FeAsO_4 \cdot 2H_2O$	1.3303	1.01406
0.0307	0.0000	$FeAsO_4 \cdot 2H_2O$	1.3322	1.03038
0.0445	0.0001	$FeAsO_4 \cdot 2H_2O$	1.3328	1.03338
0.1073	0.0001	$FeAsO_4 \cdot 2H_2O$	1.3445	1.11878
0.1611	0.0002	$FeAsO_4 \cdot 2H_2O$	1.3587	1.20135
0.1734	0.0003	$FeAsO_4 \cdot 2H_2O$	1.3600	1.23900
0.2428	0.0025	$FeAsO_4 \cdot 2H_2O$	1.3926	1.42565
0.2930[a]	**0.0132**	**$FeAsO_4 \cdot 2H_2O$ + $Fe(H_2AsO_4)_3 \cdot 5H_2O$**	**1.4096**[a]	**1.73061**[a]
0.2969	0.0181	$Fe(H_2AsO_4)_3 \cdot 5H_2O$	1.4135	1.55187
0.3529	0.0111	$Fe(H_2AsO_4)_3 \cdot 5H_2O$	1.4217	1.67222
0.4273	0.0064	$Fe(H_2AsO_4)_3 \cdot 5H_2O$	1.4571	1.97641
0.4634	0.0045	$Fe(H_2AsO_4)_3 \cdot 5H_2O$	1.4798	2.17227
0.4928	0.0034	$Fe(H_2AsO_4)_3 \cdot 5H_2O$	1.4903	2.28030

[a] Data from curve fit to eqs 2 and 3.

Table 3. Parameters of Equation 1 for Solubility Fit for Different Solid Phases at (323.15 and 343.15) K[a]

β_1^i	β_2^i	β_3^i	β_4^i	β_5^i	AAD
		$FeAsO_4 \cdot 2H_2O$			
		323.15 K			
0.0013	−0.1011	2.6263	−27.2601	98.4525	$2.86 \cdot 10^{-06}$
		$FeAsO_4 \cdot 2H_2O$			
		343.15 K			
0.0001	−0.0009	0.0597	−0.8054	3.0585	$1.62 \cdot 10^{-06}$
		$Fe(H_2AsO_4)_3 \cdot 5H_2O$			
		323.15 K			
0.0579	−0.4530	0.9836	0.1256	−1.4856	$3.76 \cdot 10^{-05}$
		$Fe(H_2AsO_4)_3 \cdot 5H_2O$			
		343.15 K			
1.3924	−13.7111	50.9869	−83.9818	51.4827	$2.01 \cdot 10^{-06}$

[a] AAD = $|\Sigma(s^{exp} - s^{cal})/n|$, where n is the number of experimental points.

Demopoulos et al.[7] obtained crystalline scorodite under ambient pressure at temperatures over the range (353.15 to 363.15) K employing a supersaturation-controlled precipitation procedure from chloride solutions containing 2 g·L^{-1} As(V) and a variable Fe(III)/As(V) molar ratio (1/1, 2/1, and 4/1). The maximum neutralization used at 368.15 K was 18 mmol NaOH·L^{-1}·min^{-1}. Lowering the temperature to 353.15 K necessitated even lower supersaturation and lower neutralization rates for crystalline scorodite to be produced. In the absence of supersaturation control, homogeneous nucleation was found to prevail, and amorphous ferric arsenate was produced. Without seeding, crystalline scorodite production by this method was only possible at 368.15 K.

Singhania et al.[8] presented an extensive program of scorodite precipitation tests under ambient pressure which showed that the rate of scorodite formation increases dramatically from a small increase in temperature from (353.15 to 373.15) K. The beneficial effects of temperature are attributed to the higher thermodynamic stability of scorodite at elevated temperatures but also to higher rates of secondary nuclei formation and crystal growth.

Fujita et al.[9] studied the effects of reaction temperature [(368.15, 343.15, and 323.15) K] and the oxidizing agent (air, pure oxygen gas) to optimize scorodite formation in a practical process. Their results indicate that controlled synthesis at 343.15 K achieved sufficiently stable scorodite particles and that air oxidation produced scorodite even at 323.15 K. The final concentration of arsenic at 343.15 K was the same as that at 368.15 K. A reaction temperature of 323.15 K was not sufficient. The results indicated that very fine crystals formed at 323.15 K that agglomerate to produce larger-sized particles, while at higher temperatures, the smaller particles are more crystalline and discrete.

Swash and Monhemius[10] studied calcium arsenates and found that at temperatures of less than 373.15 K and pH 6, crystalline hydrates of $CaHAsO_4$ form, such as haidingerite ($CaHAsO_4 \cdot H_2O$), which forms at 323.15 K, and pharmacolite ($CaHAsO_4 \cdot 2H_2O$), which forms at 293.15 K. At temperatures higher than 373.15 K, the solids have little water of hydration, consequently weilita forms ($CaHAsO_4$). TCLP tests conducted on these calcium arsenates show that they are soluble in water, with an arsenic lixiviation range of (900 to 4400) mg·L^{-1}, which is not a good indicator to immobilize arsenic.

Moon et al.[11] worked with a calcium−arsenic system with different molar ratios (1, 1.5, 2, 2.5, and 4) at 293.15 K. The arsenic concentration in solution was very high (5165 mg·L^{-1}), in molar ratios of Ca/As of 1, but decreased significantly to 1.5 mg·L^{-1} at a molar ratio of Ca/As of 4. The immobilization of As(V) was more pronounced at molar ratios of Ca/As greater than or equal to 2.5.

Bothe and Brown[12] studied the mixing of $Ca(OH)_2$, H_3AsO_4, and deionized water at room temperature (296.15 K). At Ca/As molar ratios between 2 and 2.5, $Ca_4(OH)_2(AsO_4)_2 \cdot 4H_2O$ forms, with arsenic concentrations of less than 0.5 mg·L^{-1}, reaching 0.01 mg·L^{-1} at a pH close to 12.5. At molar ratios of Ca/As between 1.5 and 2 and pH between 7 and 12, $Ca_3(AsO_4)_2 \cdot 4H_2O$ is formed. If the pH is over 9, the structure corresponds to $Ca_3(AsO_4)_2 \cdot 3^2/_3H_2O$ with an arsenic concentration in the equilibrium solution less than 0.17 mg·L^{-1} at a pH over 11. If the pH is below 9, the water increases in the crystal structure, forming $Ca_3(AsO_4)_2 \cdot 4^1/_4H_2O$. The arsenic concentrations in equilibrium were high, which indicates that it is not a good structure to immobilize arsenic, unlike the two mentioned previously.

In the mining industry, compounds containing Fe(III) + As(V) or Ca(II) + As(V), in an aqueous medium, are currently considered to be the most suitable forms for arsenic disposal. Because of this, to employ crystallization as a separation medium of toxic arsenical residues it is necessary to have basic information about the solubility and physical properties of these compounds in solution. With the objective of contributing to

Table 4. Values for the Parameters in Equations 2 and 3 for Density and Refractive Index for Each Solid Phase at (323.15 and 343.15) K

property	solid phase	β_1^j	β_2^j	β_3^j	β_4^j	AAD
			323.15 K			
ρ (g·cm^{-3})	$FeAsO_4 \cdot 2H_2O$	0.9881	1.6389	1.7002	−3.1178	0.0105
	$Fe(H_2AsO_4)_3 \cdot 5H_2O$	0.9881	1.5229	1.9056	−1.5852	0.0193
n_D	$FeAsO_4 \cdot 2H_2O$	1.3289	0.1201	1.2037	−2.4538	0.0023
	$Fe(H_2AsO_4)_3 \cdot 5H_2O$	1.3289	0.1868	0.2527	1.1933	0.0038
			343.15 K			
ρ (g·cm^{-3})	$FeAsO_4 \cdot 2H_2O$	0.97779	1.2823	0.4928	43.7392	0.0087
	$Fe(H_2AsO_4)_3 \cdot 5H_2O$	0.97779	−0.6244	6.5733	9.6897	0.0135
n_D	$FeAsO_4 \cdot 2H_2O$	1.3251	0.1137	0.6229	0.4733	0.0012
	$Fe(H_2AsO_4)_3 \cdot 5H_2O$	1.3251	−0.0680	0.8028	2.0455	0.0022

this type of information, in previous work we reported data on the solubility, density, and refractive index of the system $Fe_2(SO_4)_3 + As_2O_5 + H_2O$ at temperatures of (323.15 and 343.15) K.[13] Continuing with this objective, in this work a similar study was made of the systems $As_2O_5 + Fe(OH)_3 + H_2O$ and $As_2O_5 + CaCO_3 + H_2O$. It is important to point out that in the study of the first system, prior to each experiment, ferric hydroxide was obtained through the reaction of NaOH and $Fe_2(SO_4)_3 \cdot 5H_2O$, because active $Fe(OH)_3$ is required, since the commercial reagent does not complete this condition.

2. Experimental Section

2.1. Materials. Analytical grade reagents ($As_2O_5 \cdot 3H_2O$, Sigma Aldrich, 98 %; $CaCO_3$, Merck, 99 %; NaOH, Merck, 99 %; $Fe_2(SO_4)_3 \cdot 5H_2O$, Riedel-De Haën, (21 to 23) % Fe) were used in the experiments along with ultrapure water (conductivity $\leq 0.05\ \mu S \cdot cm^{-1}$) obtained by passing distilled water through a Millipore Co. "Ultrapure Cartridge Kit". All reagents were used as received commercially without any additional purification.

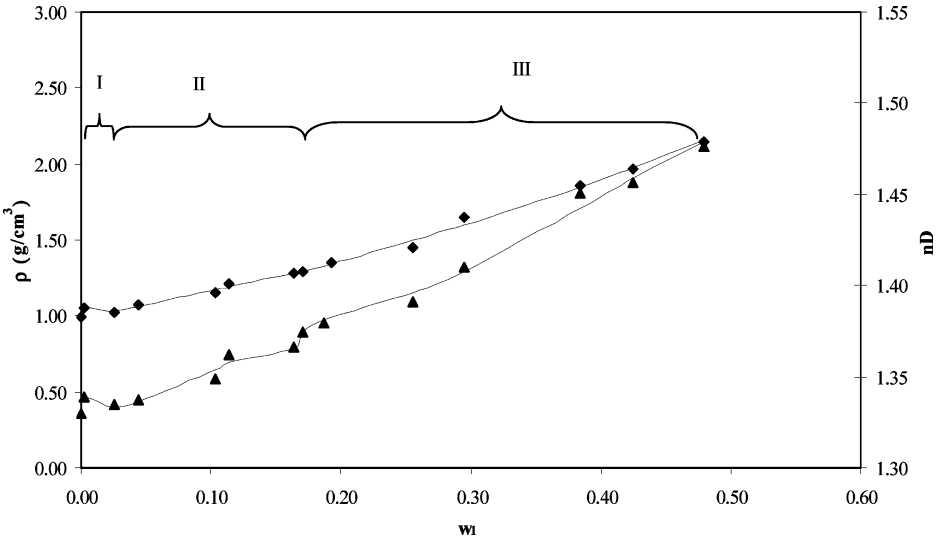

Figure 1. Experimental values (solid symbols) and correlations of ◆, density and ▲, refractive index versus arsenic (As) mass fraction for the $As_2O_5 + Fe(OH)_3 + H_2O$ system at 323.15 K. I, II, and III represent the crystallization fields $FeSO_4(OH)(H_2O)_2$, $FeAsO_4 \cdot 2H_2O$, and $Fe(H_2AsO_4)_3 \cdot 5H_2O$, respectively.

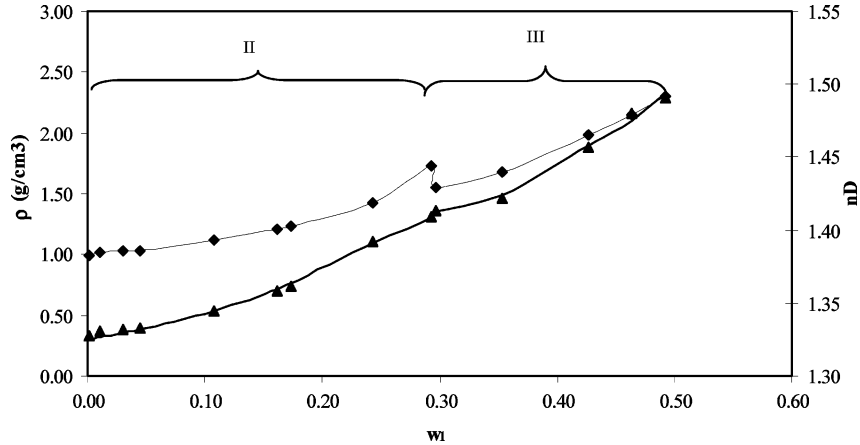

Figure 2. Experimental values and correlations of ◆, density and ▲, refractive index versus arsenic (As) mass fraction for the $As_2O_5 + Fe(OH)_3 + H_2O$ system at 343.15 K. II and III represent the crystallization fields $FeAsO_4 \cdot 2H_2O$ and $Fe(H_2AsO_4)_3 \cdot 5H_2O$, respectively.

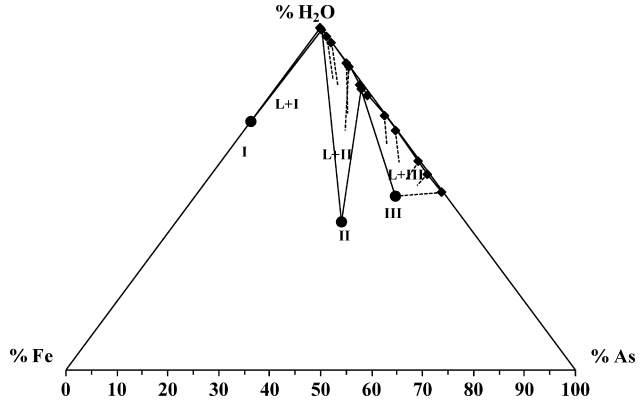

Figure 3. Phase diagram for the As(V) + Fe(III) + H_2O system in ferric mass fraction (w_2) versus arsenic mass fraction (w_1) at 323.15 K. Solid symbols represent the solubility equilibrium data. Dotted lines represent the results of the wet-residue method. Solid circles represent the two precipitated salts in the solubility study. Crystallization fields are indicated.

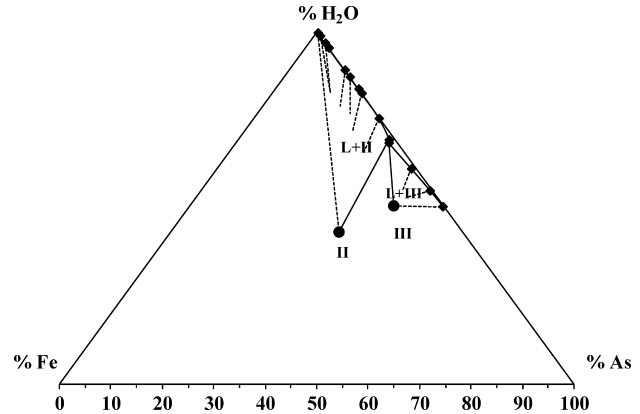

Figure 4. Phase diagram for the As(V) + Fe(III) + H_2O system in ferric mass fraction (w_2) versus arsenic mass fraction (w_1) at 343.15 K. Solid symbols represent the solubility equilibrium data. Dotted lines represent the results of the wet-residue method. Solid circles represent the two precipitated salts in the solubility study. Crystallization fields are indicated.

Table 5. Solubility, *w* (Mass Fraction), of As(1) and Ca(2), Refractive Index, n_D, and Density, ρ, for the As_2O_5 + $CaCO_3$ + H_2O System at 323.15 K

w_1	w_2	solid phase	n_D	ρ (g·cm^{-3})
0.0000	0.0001	$CaHAsO_4 \cdot H_2O$	1.3289	0.98874
0.0017	0.0010	$CaHAsO_4 \cdot H_2O$	1.3298	0.99395
0.0027	0.0011	$CaHAsO_4 \cdot H_2O$	1.3300	0.99405
0.0502	0.0132	$CaHAsO_4 \cdot H_2O$	1.3427	1.06501
0.0853	0.0217	$CaHAsO_4 \cdot H_2O$	1.3540	1.13339
0.1335	0.0331	$CaHAsO_4 \cdot H_2O$	1.3723	1.25172
0.1600[a]	**0.0483**	**$CaHAsO_4 \cdot H_2O$ + $Ca(H_2AsO_4)_2$**	**1.3889**[a]	**1.35401**[a]
0.2066	0.0473	$Ca(H_2AsO_4)_2$	1.3966	1.42230
0.269	0.0341	$Ca(H_2AsO_4)_2$	1.4098	1.54590
0.3038	0.0251	$Ca(H_2AsO_4)_2$	1.41982	1.64290
0.3133	0.0249	$Ca(H_2AsO_4)_2$	1.42037	1.65040
0.3844	0.0127	$Ca(H_2AsO_4)_2$	1.4377	1.82110
0.4035	0.0113	$Ca(H_2AsO_4)_2$	1.4443	1.87150
0.4592	0.0000	$Ca(H_2AsO_4)_2$	1.3289	2.23010

[a] Data from curve fit to eqs 5 and 6.

2.2. Apparatus and Procedures. 2.2.1. Solid−Liquid Equilibrium. In the study of the first system (As_2O_5 + $Fe(OH)_3$ + H_2O), known masses of water, arsenic pentoxide, and ferric hydroxide, the two latter being in excess to ensure the saturation of the solutions, were measured on a Mettler Toledo Co. model AX204 analytical balance with a precision of 0.07 mg. In the study of the second system (As_2O_5 + $CaCO_3$ + H_2O), the procedure was analogous, only now adding arsenic pentoxide and calcium carbonate in excess.

Table 6. Solubility, *w* (Mass Fraction), of As(1) and Ca(2), Refractive Index, n_D, and Density, ρ, for the As_2O_5 + $CaCO_3$ + H_2O System at 343.15 K

w_1	w_2	solid phase	n_D	ρ (g·cm^{-3})
0.0040	0.0011	$CaHAsO_4 \cdot H_2O$	1.3265	0.98553
0.0880	0.0239	$CaHAsO_4 \cdot H_2O$	1.3544	1.17307
0.1330	0.0316	$CaHAsO_4 \cdot H_2O$	1.3641	1.25251
0.1740	0.0366	$CaHAsO_4 \cdot H_2O$	1.3836	1.33807
0.2180	0.0439	$CaHAsO_4 \cdot H_2O$	1.3972	1.42391
0.2189[a]	**0.0442**	**$CaHAsO_4 \cdot H_2O$ + $Ca(H_2AsO_4)_2$**	**1.3977**[a]	**1.41684**[a]
0.2280	0.0437	$Ca(H_2AsO_4)_2$	1.3997	1.42381
0.3220	0.0250	$Ca(H_2AsO_4)_2$	1.4206	1.63462
0.4060	0.0133	$Ca(H_2AsO_4)_2$	1.4404	1.84413
0.4830	0.0022	$Ca(H_2AsO_4)_2$	1.4705	2.12281

[a] Data from curve fit to eqs 5 and 6.

Table 7. Parameter of Equation 4 for Solubility Fits for Different Solid Phases at (323.15 and 343.15) K[a]

β_1^j	β_2^j	β_3^j	β_4^j	AAD
		$CaHAsO_4 \cdot H_2O$		
		323.15 K		
0.0002	0.3540	−1.9975	8.9429	0.0002
		$CaHAsO_4 \cdot H_2O$		
		343.15 K		
−0.0004	0.3773	−1.3793	2.5083	0.0001
		$Ca(H_2AsO_4)_2$		
		323.15 K		
0.0303	0.4879	−2.6316	3.2364	0.0003
		$Ca(H_2AsO_4)_2$		
		343.15 K		
0.1561	−0.8076	1.7048	−1.4328	0.00003

[a] AAD = $|\Sigma(s^{exp} - s^{cal})/n|$, where n is the number of experimental points.

A rotatory thermostatic (to ± 0.1 K) water bath with a holder for eight 40 mL glass jars was used to obtain data on phase equilibria at (323.15 and 343.15) K. The samples were stirred for 7 days for the first system and 5 days for the second system to reach equilibrium at the desired temperature. Once equilibrium was reached, agitation was stopped, and the samples were left decanting for a period of 6 h. The clear supernatant liquid was collected from the flasks and filtered using Whatman membrane filters (GD/X, 25 mm) with a nominal pore size of 0.45 μm.

The agitation time of 7 and 5 days was determined in work prior to the experimental study. This work consisted of preparing various solutions of only one concentration, the refraction index of which was measured periodically (every 24 h) until this property reached a constant.[14−16] Measuring the agitation time elapsed in this study allowed the adequate agitation time to be defined to reach the phase equilibrium conditions of each system.

The experimental procedure to determine the concentrations of ferric and arsenic has already been described in previous work.[13] The procedure to determine the concentration of calcium is similar, except that the samples and standards for this analysis were made under final acidity conditions of 5 % HCl, plus the addition of lanthanum. Calcium concentrations were determined by double beam atomic absorption spectrometry (AA), at a wavelength of 422.7 nm with an acetylene-nitrous oxide flame, using a Varian model SpectrAA 220 instrument.

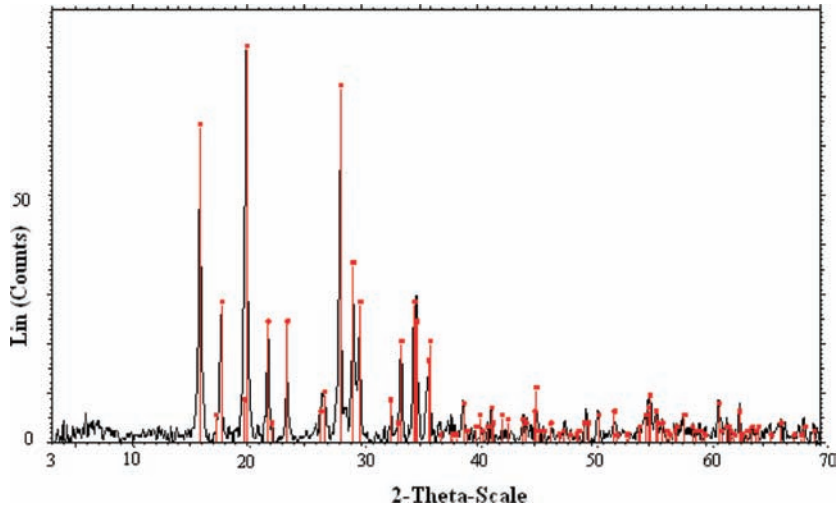

Figure 5. Diffractogram of solid sample obtained in the crystallization field of the scorodite at 343.15 K. Lin represents the number of count over the Scintillometer denoting intensity and function of the 2-θ rotating angle. Black line represents the sample synthesized in the experiment. Red line represents the scorodite pattern from database.

Table 8. Values for the Parameters in Equations 5 and 6 for Density and Refractive Index for Each Solid Phase at (323.15 and 343.15) K[a]

property	solid phase	β_1^j	β_2^j	β_3^j	β_4^j	AAD
			323.15 K			
ρ (g·cm^{-3})	$CaHAsO_4 \cdot H_2O$	0.9881	−0.5244	6.4946	6.5831	0.0007
	$Ca(H_2AsO_4)_3$	0.9881	1.8346	0.8487	0.3394	0.0049
n_D	$CaHAsO_4 \cdot H_2O$	1.3289	−0.0606	0.7891	1.1300	0.00001
	$Ca(H_2AsO_4)_3$	1.3289	0.2640	0.0342	0.2426	0.0008
			343.15 K			
ρ (g·cm^{-3})	$CaHAsO_4 \cdot H_2O$	0.9778	1.4522	0.3812	2.5459	0.0027
	$Ca(H_2AsO_4)_3$	0.9778	0.7469	3.3132	2.4275	0.0090
n_D	$CaHAsO_4 \cdot H_2O$	1.3251	0.3362	0.0953	−0.1291	0.0017
	$Ca(H_2AsO_4)_3$	1.3251	0.1344	0.3347	0.6179	0.0015

[a] AAD = $|\Sigma(s^{exp} - s^{cal})/n|$, where n is the number of experimental points.

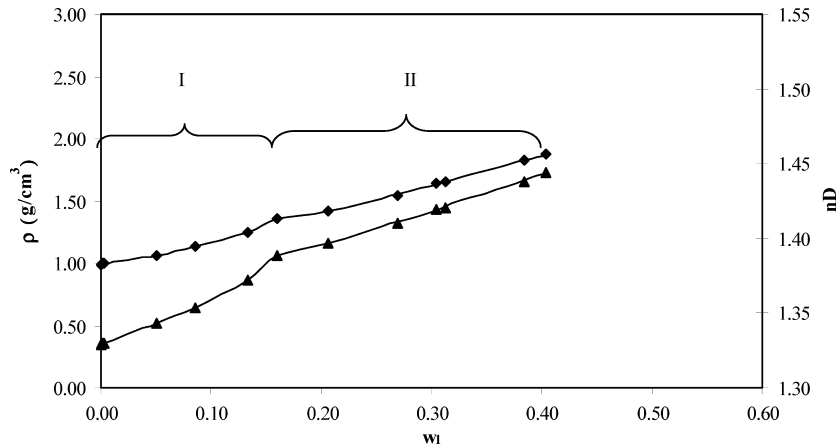

Figure 6. Experimental values and correlations of ◆, density and ▲, refractive index versus arsenic (As) mass fraction (w_1), for the $As_2O_5 + CaCO_3 + H_2O$ system at 323.15 K. I and II represent the crystallization fields $CaHAsO_4 \cdot H_2O$ and $Ca(H_2AsO_4)_2 \cdot 5H_2O$, respectively.

In all cases, the experiments were performed in duplicate for each composition, obtaining a standard mean deviation (in fractional mass) of 0.26 % and 0.036 % for As and Fe, respectively, for the system $As_2O_5 + Fe(OH)_3 + H_2O$. For the $As_2O_5 + CaCO_3 + H_2O$ system, the result was 0.56 % and 0.051 % for As and Ca, respectively.

The precipitated solids were studied by X-ray diffraction and Scanning Electron Microscopy (SEM) analysis. SEM analysis was conducted using a Jeol 6260 LV, and XRD measurement was performed on a Siemens D5000.

2.2.2. Physical Properties. Density measurements were carried out in triplicate using a Mettler-Toledo model DE50 oscillation densimeter, with a resolution of $\pm\ 1 \cdot 10^{-5}$ g·cm^{-3}. The temperature was thermostatically controlled to (323.15 and 343.15 $\pm$ 0.1) K by means of a self-contained Peltier system provided with the densimeter. Density values represent the average of between two independent experiments, with the measured values being reproducible to within $\pm\ 3.44 \cdot 10^{-5}$ g·cm^{-3} and $\pm\ 1.55 \cdot 10^{-5}$ g·cm^{-3} for the first and second system, respectively.

The refractive index of each solution was determined using a Mettler-Toledo model RE40 refractometer with a resolution of $\pm\ 1 \cdot 10^{-4}$. The measurements were repeated at least three times with no appreciable variation. As in the case of the

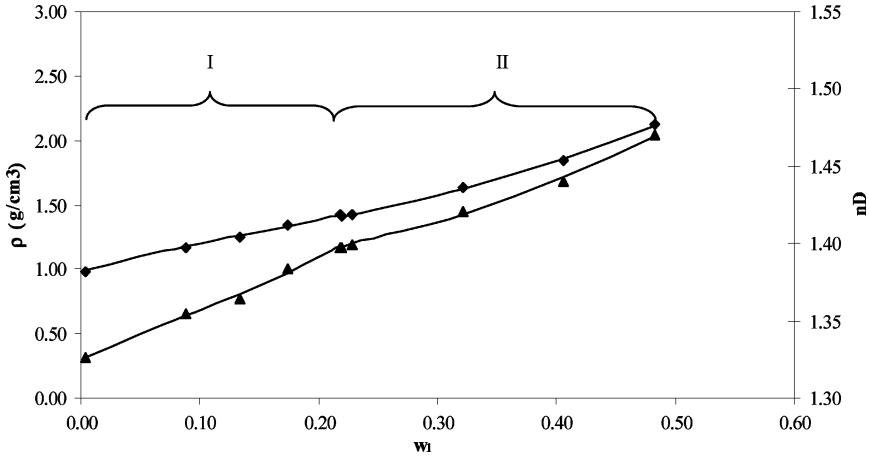

Figure 7. Experimental values and correlations of ◆, density and ▲, refractive index versus arsenic (As) mass fraction (w_1), for the $As_2O_5 + CaCO_3 + H_2O$ system at 343.15 K. I and II represent the crystallization fields $CaHAsO_4 \cdot H_2O$ and $Ca(H_2AsO_4)_2 \cdot 5H_2O$, respectively.

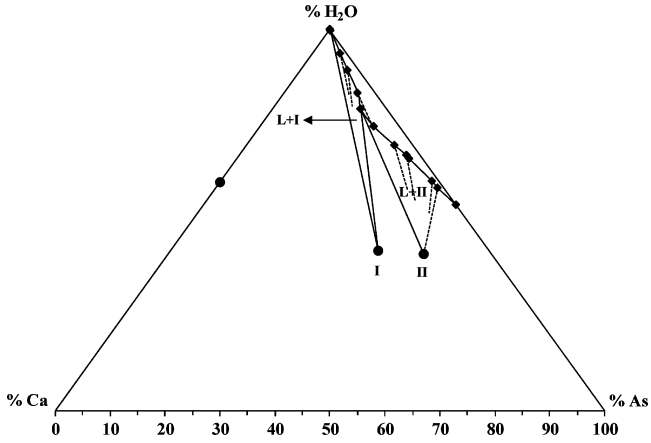

Figure 8. Phase diagram for the As(V) + Ca + H_2O system in calcium mass fraction (w_2) versus arsenic mass fraction (w_1) at 323.15 K. Solid symbols represent the solubility equilibrium data. Dotted lines represent the results of the wet-residue method. Solid circles represent the two precipitated salts in the solubility study. Crystallization fields are indicated.

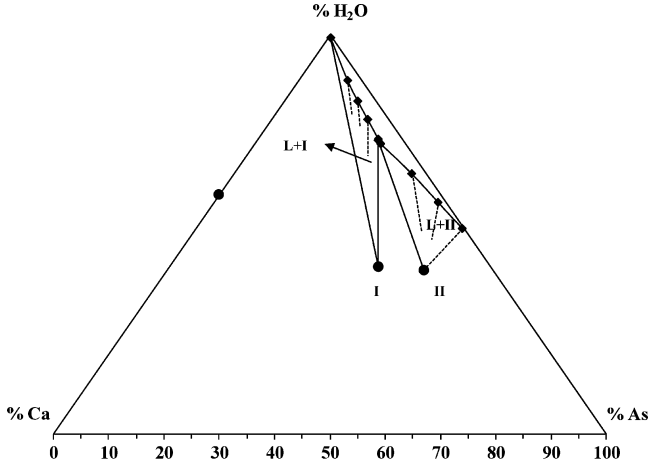

Figure 9. Phase diagram for the As(V) + Ca + H_2O system in calcium mass fraction (w_2) versus arsenic mass fraction (w_1) at 343.15 K. Solid symbols represent the solubility equilibrium data. Dotted lines represent the results of the wet-residue method. Solid circles represent the two precipitated salts in the solubility study. Crystallization fields are indicated.

densimeter, the refractometer temperature was controlled to (323.15 and 343.15 ± 0.1) K by a self-contained Peltier system. Refractive index values represent the average of two independent experiments, with the measured values being reproducible to within ± $4.76 \cdot 10^{-4}$ and ± $1.76 \cdot 10^{-4}$ for the first and second system, respectively.

A TLCP test[17] was carried out on the crystals obtained to determine the stability and to evaluate if they are potentially interesting as alternative waste materials in industrial processes. The TCLP test establishes standards in terms of limits of concentration. This procedure consists of leaching a solid sample for 18 h in a weak solution of acetic acid in a liquid/solid proportion of 20:1, with agitation of 30 rpm and a temperature of 295.15 K. Once the test is completed, the filtered solution is analyzed, and this should not exceed 5 $mg \cdot L^{-1}$ of arsenic to be considered a stable solid.

3. Results and Discussion

3.1. $As_2O_5 + Fe(OH)_3 + H_2O$ Ternary System. 3.1.1. Solubility at (323.15 and 343.15) K and Empirical Fit. The results of the solubility of the $As_2O_5 + Fe(OH)_3 + H_2O$ system at (323.15 and 343.15) K, expressed as fractional mass of arsenic and ferric, are shown in Tables 1 and 2. The pH variation of the solutions was in a range between 0 and 11, noting that for high concentrations of arsenic the pH was close to 0. Atomic absorption and X-ray diffraction analyses confirmed that the salts at equilibrium were those indicated in Tables 1 and 2 (see Section 3.1.3). The double equilibrium points where the liquid is in equilibrium with two different solid phases was obtained from fits of liquid curves of the two crystallization fields, using empirical equations. The experimental confirmation of the previous procedure is detailed later for the $As_2O_5 + CaCO_3 + H_2O$ system (see Section 3.2.3).

For (323.15 and 343.15) K, the values for the ferric mass fraction (w_2) at saturation were correlated as a function of the arsenic mass fraction (w_1) for the different crystallization fields, according to eq 1

$$w_2 = \beta_1^j + \beta_2^j \cdot (w_1) + \beta_3^j \cdot (w_1)^2 + \beta_4^j \cdot (w_1)^3 + \beta_5^j \cdot (w_1)^4 \quad (1)$$

where β_i^j (with $i = 1$ to 5, j is the crystallization field I, II, or III) are empirical coefficients. The symbols I, II, and III represent the crystallization fields of $FeSO_4(OH)(H_2O)_2$ (parabluterite), $FeAsO_4 \cdot 2H_2O$ (scorodite), and $Fe(H_2AsO_4)_3 \cdot 5H_2O$ (kaatialaite), respectively. The optimized values for coefficients in eq 1 and the average absolute deviation (AAD) between all the calculated and experimental values are presented in Table 3.

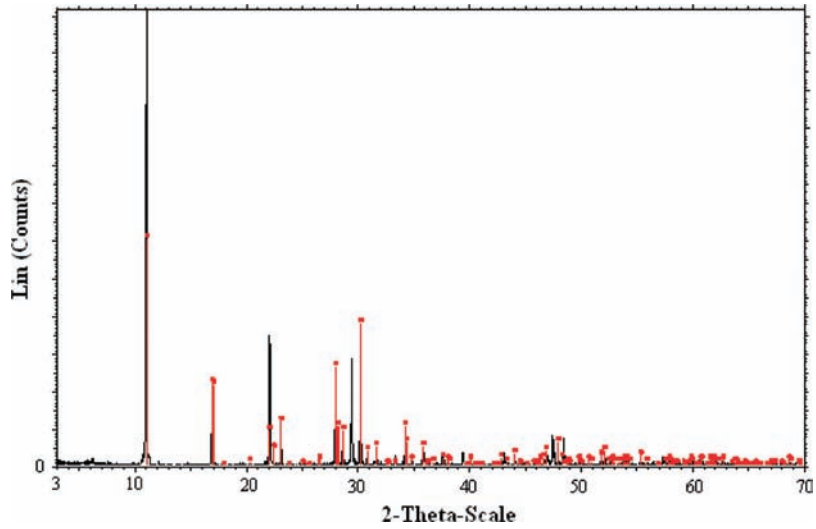

Figure 10. Diffractogram of solid sample obtained in the crystallization field of the haidingerite at 343.15 K. Lin represents the number of count over the Scintillometer denoting intensity and function of the 2-θ rotating angle. Black line represents the sample synthesized in the experiment. Red line represents the haidingerite pattern from database.

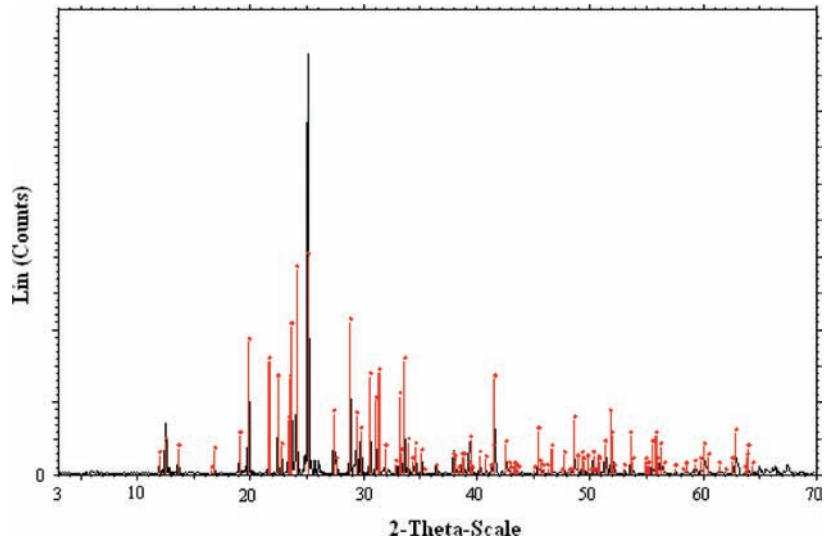

Figure 11. Diffractogram of solid sample obtained in the crystallization field of the svenekite at 343.15 K. Lin represents the number of count over the Scintillometer denoting intensity and function of the 2-θ rotating angle. Black line represents the sample synthesized in the experiment. Red line represents the svenekite pattern from database.

3.1.2. Physical Properties at (323.15 and 343.15) K and Empirical Fit. In Tables 1 and 2, the densities and refractive index of the saturated solutions of the $As_2O_5 + Fe(OH)_3 + H_2O$ system are presented. For (323.15 and 343.15) K, the values for density (ρ) and refractive index (n_D) were correlated as a function of the arsenic mass fraction (w_1) and ferric mass fraction (w_2) for the different crystallization fields, following eqs 2 and 3

$$\rho/(g \cdot cm^{-3}) = \beta_1^j + \beta_2^j \cdot (w_1) + \beta_3^j \cdot (w_1)^2 + \beta_4^j \cdot (w_2) \quad (2)$$

$$n_D = \beta_1^j + \beta_2^j \cdot (w_1) + \beta_3^j \cdot (w_1)^2 + \beta_4^j \cdot (w_2) \quad (3)$$

where β_i^j ($i = 1$ to 4, $j =$ I, II, or III) are empirical coefficients. In Table 4, the optimized values for coefficients in eqs 2 and 3 and the average absolute deviation (AAD) between all the calculated and experimental values are presented.

These results shown in Figures 1 and 2 confirm a good general adjustment of the experimental values of the physical properties study (density and refraction index) versus fractions of ferric and arsenical mass. By intersection of the fitted equations for both crystallization fields at 323.15 K, it was shown that when the fraction in arsenic weight was 0.0060 a mixture of salts of $FeSO_4(OH)(H_2O)_2 + FeAsO_4 \cdot 2H_2O$ is formed with a refractive index of 1.3312 and density of 0.99860 $g \cdot cm^{-3}$, and when the fraction in weight of arsenic is 0.1710, a mixture of salts of $FeAsO_4 \cdot 2H_2O + Fe(H_2AsO_4)_3 \cdot 5H_2O$ is formed with a refraction index of 1.3748 and a density of 1.29089 $g \cdot cm^{-3}$. For a temperature of 343.15 K, it was observed that when the fraction in weight of arsenic is 0.2930, a mixture of salts of $FeAsO_4 \cdot 2H_2O + Fe(H_2AsO_4)_3 \cdot 5H_2O$ is formed with a refraction index of 1.4096 and a density of 1.73061 $g \cdot cm^{-3}$.

3.1.3. Phase Diagram at (323.15 and 343.15) K. Figures 3 and 4 show the phase diagram for the As(V) + Fe(III) + H_2O system at (323.15 and 343.15) K. Curves following solid symbols represent the experimental data obtained in this work. These curves are obtained by drawing straight lines through these experimental points. Dotted lines represent values obtained using the wet-residue method.[18] Extrapolating, these lines clearly converge on the scorodite and kaatialaite. As mentioned in the

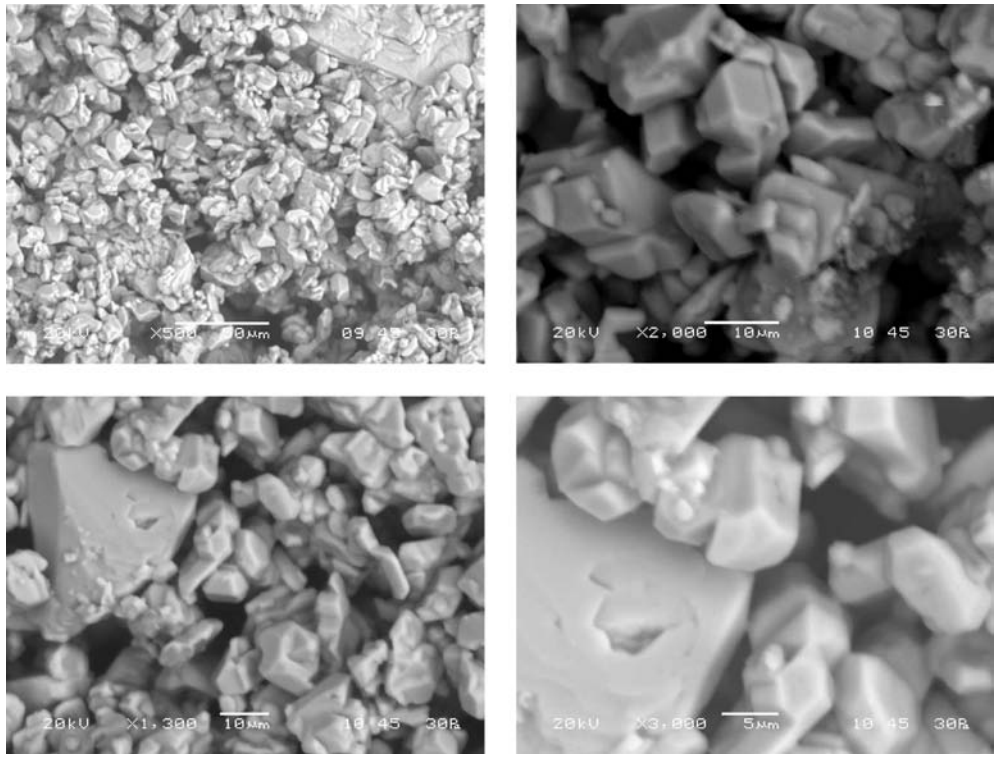

Figure 12. SEM picture of precipitated mixed phases $CaHAsO_4 \cdot H_2O + Ca(H_2AsO_4)_2$.

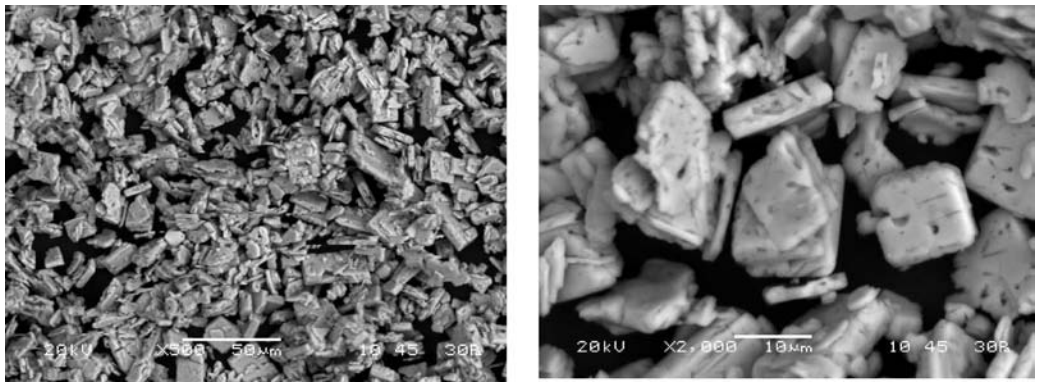

Figure 13. SEM images of $CaHAsO_4 \cdot H_2O$.

solubility study, additional X-ray diffraction experiments confirmed the identities of the salts at equilibrium.

Figure 5 shows a diffractogram corresponding to a solid sample obtained on the basis of the phase equilibrium, for the field of crystallization of the scorodite at 343.15 K. The black line corresponds to the experimental sample, whereas the red line corresponds to the pattern of crystalline scorodite obtained from the database of the X-ray diffractometer used. The figure shows that the peaks of both lines overlap, which confirms the formation of scorodite.

Three crystallization fields can be observed in Figure 3 and two in Figure 4. The letters L, I, II, and III denote the liquid and solid $FeSO_4(OH)(H_2O)_2$ (parabluterite), $FeAsO_4 \cdot 2H_2O$ (scorodite), and $Fe(H_2AsO_4)_3 \cdot 5H_2O$ (kaatialaite) phases, respectively, which form progressively as the arsenic concentration increases. The field of crystallization of scorodite is beside the field of crystallization of kaatialaite, which is in accord with Zhu et al.[19] They found that during the dissolution under strong acid conditions (pH < 2), scorodite ($FeAsO_4 \cdot 2H_2O$) can also change into kaatialaite ($Fe(H_2AsO_4)_3 \cdot 5H_2O$) that is more stable than scorodite under strong acid conditions. The liquid zone in the phase diagram is almost nonexistent. In general, the diagram is composed of solid mixtures and the mentioned salts.

At the temperature of 323.15 K, the crystallization field of the scorodite is slightly smaller than the field at 343.15 K. The mass fraction of As oscillates between 0.006 and 0.1710 for 323.15 K and between 0.0017 and 0.2930 at 343.15 K. At 323.15 K, in the first zone the solutions are saturated in the salt (I), next to the H_2O−Fe axis, while in the second the zones are saturated in the salt (II) and the third zone is saturated in the salt (III). Phase I disappears at 343.15 K. In these figures, the experimental values (represented by discrete values) are the result of an average of two measurements made separately.

3.1.4. Toxicity Characteristic Leaching Procedure. The results of the TCLP lixiviation indicated that the kaatialaite is not a good option for disposition, owing to its relatively high solubility of 5100 $mg \cdot L^{-1}$ of As in weak acetic acid (0.004 M) and 5400 $mg \cdot L^{-1}$ of As in distilled water.

For the scorodite, the TCLP test had a result of 400 $mg \cdot L^{-1}$ of As at a temperature of 323.15 K and of 100 $mg \cdot L^{-1}$ of As at a temperature of 343.15 K.

3.2. $As_2O_5 + CaCO_3 + H_2O$ Ternary System. 3.2.1. Solubility at (323.15 and 343.15) K and Empirical Fit. The results of the solubility of the $As_2O_5 + CaCO_3 + H_2O$ system at (323.15 and 343.15) K, expressed as fractional mass of arsenic and calcium are shown in Tables 5 and 6. The pH of the solution was always between 1 and 7 at 323.15 K, while at 343.15 K it varies between 0 and 5. It was observed that when the arsenic content reached high values, pH values became closer to zero. Atomic absorption and X-ray diffraction analyses confirmed that the salts at equilibrium were those indicated in Tables 5 and 6.

For (323.15 and 343.15) K, the values for the calcium mass fraction (w_2) at saturation were correlated as a function of the arsenic mass fraction (w_1) for the different crystallization fields, according to eq 4

$$w_2 = \beta^j_1 + \beta^j_2 \cdot (w_1) + \beta^j_3 \cdot (w_1)^2 + \beta^j_4 \cdot (w_1)^3 + \beta^j_5 \cdot (w_1)^4 \quad (4)$$

where β^j_i (with $i = 1$ to 5, j is the crystallization field I or II) are empirical coefficients. The symbols I and II represent the crystallization field of $CaHAsO_4 \cdot H_2O$ (haidingerite) and $Ca(H_2AsO_4)_2$ (svenekite), respectively. The optimized values for coefficients in eq 4 and the average absolute deviation (AAD) between all the calculated and experimental values are presented in Table 7.

3.2.2. Physical Properties at (323.15 and 343.15) K and Empirical Fit. Tables 5 and 6 present the densities and refractive index of the saturated solutions of the $As_2O_5 + CaCO_3 + H_2O$ system. For (323.15 and 343.15) K, the values for density (ρ) and refractive index (n_D) were correlated as a function of the arsenic mass fraction (w_1) and calcium mass fraction (w_2) for the different crystallization fields, following eqs 5 and 6

$$\rho/(g \cdot cm^{-3}) = \beta^j_1 + \beta^j_2 \cdot (w_1) + \beta^j_3 \cdot (w_1)^2 + \beta^j_4 \cdot (w_2) \quad (5)$$

$$n_D = \beta^j_1 + \beta^j_2 \cdot (w_1) + \beta^j_3 \cdot (w_1)^2 + \beta^j_4 \cdot (w_2) \quad (6)$$

where β^j_i ($i = 1$ to 4, $j =$ I or II) are empirical coefficients. In Table 8, the optimized values for coefficients in eqs 5 and 6 and the average absolute deviation (AAD) between all the calculated and experimental values are presented. The results are shown in Figures 6 and 7.

By intersection of the fitted equations for both crystallization fields at 323.15 K, it was shown that when the fraction in arsenic weight was 0.1600 a mixture of salts of $CaHAsO_4 \cdot H_2O$ (haidingerite) and $Ca(H_2AsO_4)_2$ (svenekite) is formed with a refractive index of 1.3889 and density of 1.35401 $g \cdot cm^{-3}$. For a temperature of 343.15 K, the same mix of salts is formed, when the fraction in weight of arsenic is 0.2189. The refraction index and the density of this double equilibrium point are, respectively, (1.3977 and 1.41684) $g \cdot cm^{-3}$.

3.2.3. Phase Diagram at (323.15 and 343.15) K. Figures 8 and 9 show the phase diagram for the As(V) + Ca + H_2O system at (323.15 and 343.15) K. Curves following solid symbols represent the experimental data obtained in this work. These curves are obtained by drawing straight lines through these experimental points. Dotted lines represent values obtained using the wet-residue method.[18] Extrapolation of these lines shows convergence between the arsenic and calcium salts. As mentioned in the solubility study, additional X-ray diffraction experiments confirmed the identities of the salts at equilibrium. Figures 10 and 11 show diffractograms corresponding to solid phases obtained on the basis of the phase equilibrium, for the field of crystallization of the haidingerite and svenekite at 343.15 K, respectively. The black line corresponds to the experimental sample, whereas the red line corresponds to the patterns of each salt obtained from the database of the X-ray diffractometer used. The peaks of the black and red lines are coincident in the two figures.

The letters L, I, and II denote the liquid and solid $CaHAsO_4 \cdot H_2O$ and $Ca(H_2AsO_4)_2$ phases, respectively.

At 323.15 K, two crystallization fields were observed, and the straight solid line of the fractional mass of arsenic between 0 and 0.1600 divides the liquid−solid region in two zones (L + I and L + II). In the first zone, the solutions are saturated in salt (I), while in the second zone the solutions are saturated in the salt (II). The same is observed for the system at 343.15 K. In these figures, the experimental values (represented by discrete points) are the result of an averaging of two separate measurements.

A solution (8 % Ca and 27.01 % As) was prepared inside of the double saturation field formed by the eutectic point and both salts as shown in Figure 9, to confirm the presence of a mixture of $CaHAsO_4 \cdot H_2O + Ca(H_2AsO_4)_2$ salts.

The samples were stirred for 5 days at 343.15 K. Once equilibrium was reached, agitation was stopped, and the samples were left decanting for a period of 6 h. The precipitated solids were dried at room temperature and analyzed by SEM. The salt compositions and SEM pictures (Figure 12) of the mixed phases $CaHAsO_4 \cdot H_2O + Ca(H_2AsO_4)_2$ confirmed that the precipitated samples are formed by mixtures of haidingerite and svenekite. The molar Ca/As ratios of the $CaHAsO_4 \cdot H_2O$ and $Ca(HAsO_4)_2$ are 0.6 and 0.3, respectively. The mixed phases $CaHAsO_4 \cdot H_2O + Ca(H_2AsO_4)_2$ obtained by SEM are between 0.3 and 0.5, which represents an intermediate value between the two pure salts. The crystallographic systems are orthorhombic and triclinic for haidingerite and svenekite, respectively, as shown in Figure 12.

The SEM photos (Figure 13) show a haidingerite crystal. It is possible to see the porosity formed by boiling gas (CO_2) during crystallization. Also it is possible to see the orthorhombic form which is characteristic of haidingerite.

3.2.4. Toxicity Characteristic Leaching Procedure. For haidingerite, the result of the TCLP was between (1500 to 1300) $mg \cdot L^{-1}$ of As at a temperature of 323.15 K and 1100 $mg \cdot L^{-1}$ of As at a temperature of 343.15 K. This indicates a high solubility of the solid, because of which it is not a good residue for fixing arsenic.

Glossary

List of Symbols

AAD	absolute average deviation
I	$FeSO_4(OH)(H_2O)_2$, $CaHAsO_4 \cdot H_2O$
II	$FeAsO_4 \cdot 2H_2O$, $Ca(H_2AsO_4)_2$
III	$Fe(H_2AsO_4)_3 \cdot 5H_2O$
L	liquid phase
n	number of experimental points
n_D	refractive index
TCLP	Toxicity Characteristic Leaching Procedure
w_1	mass fraction arsenic
w_2	mass fraction iron, calcium

Greek Symbols

β^j_i	empirical coefficient (j indicates phase and i indicates the number of parameters)
ρ	density

Literature Cited

(1) Woolson, E. Mercury and Arsenic Wastes: Removal, Recovery, Treatment and Disposal, *U.S. Environmental Protection Agency Pollution Technology Review*, Noyes Data Corporation, NJ, 1992.

(2) Smith, E.; Naidu, R.; Alston, A. M. *Advances in Agronomy*; Academic Press: New York, 1998.
(3) Ugarte, G. *La problemática del arsénico y su solución en los nuevos procesos hidrometalúrgicos para la producción de cobre*; Hydrocopper: Santiago, Chile, 2005; pp 403−412.
(4) Swash, P.; Monhemius, A. *The Scorodite Process: a technology for the disposal of arsenic in the 21st century. Effluent Treatment in the Mining Industry*; University of Concepcion: Chile, 1998; pp 119−161.
(5) Richmond, W.; Loan, M.; Morton, J.; Parkinson, G. Arsenic removal from aqueous solution via ferrihydrite crystallization control. *Environ. Sci. Technol.* **2004**, *38*, 2368−2372.
(6) Demopoulos, G. *Effluent treatment by crystallization. Clean Technology for the Mining Industry*; University of Concepcion: Chile, 1996.
(7) Demopoulos, G.; Droppert, D.; Van Weert, G. Precipitation of crystalline scorodite from chloride solutions. *Hydrometallurgy* **1995**, *38*, 245–261.
(8) Singhania, S.; Wang, Q.; Filippou, D.; Demopoulos, G. P. Temperature and seeding effects on the precipitation of scorodite from sulfate solutions under atmospheric-pressure conditions. *Metall. Mater. Trans. B* **2005**, *36B*, 327–333.
(9) Fujita, T.; Taguchi, R.; Abumiya, M.; Matsumoto, M.; Shibata, E.; Nakamura, T. Novel atmospheric scorodite synthesis by oxidation of ferrous sulfate solution. Part II. Effect of temperature and air. *Hydrometallurgy* **2008**, *90*, 85–91.
(10) Swash, P.; Monhemius, A. *Synthesis, characterization and solubility testing of solids in the Ca-Fe-AsO_4 system. Sudbury '95 - Mining and the Environment*; CANMET: Ottawa, Canada, 1995.
(11) Moon, D.; Dermatas, D.; Menounou, N. Arsenic immobilization by calcium-arsenic precipitates in lime treated soils. *Sci. Total Environ.* **2004**, *330*, 171–185.
(12) Bothe, J.; Brown, P. Arsenic immobilization by calcium arsenate formation. *Environ. Sci. Technol.* **1999**, *33*, 3806–3811.
(13) Taboada, M.; Castillo, P.; Flores, E.; Graber, T. The ternary system arsenic pentoxide + ferric sulphate + water: Solubility, density and refractive index of saturated solutions at 323.15 and 343.15 K. *Fluid Phase Equilib.* **2008**, *265*, 209–214.
(14) Morales, J.; Galleguillos, H.; Hernández-Luis, F. Solubility of NaF + NaX + H_2O (X = ClO_4 and NO_3) Ternary Systems and Density and Refractive Index of the Saturated Solutions at 298, 15 K. *J. Chem. Eng. Data* **2007**, *52*, 687–690.
(15) Taboada, M.; Véliz, D.; Galleguillos, H.; Graber, T. Solubility, Density, Viscosity, Electrical Conductivity, and Refractive Index of Saturated Solutions of Lithium Hydroxide in Water + Ethanol. *J. Chem. Eng. Data* **2005**, *50*, 187–190.
(16) Taboada, M.; Galleguillos, H.; Graber, T.; Bolado, S. Compositions, Densities, Conductivities and Refractive Indices of Potassium Chloride or/and Sodium Chloride + PEG 4000 + Water at 298.15 and Liquid-Liquid Equilibrium of Potassium Chloride or Sodium Chloride + PEG 4000 + Water at 333.15 K. *J. Chem. Eng. Data* **2005**, *50*, 264–269.
(17) USEPA. *Method 1311. Toxicity Characteristic Leaching Procedure.* Code of Federal Regulations, 40 CFR part 261, Appendix II, July **1991**.
(18) Taboada, M.; Galleguillos, H.; Graber, T.; Álvarez, J. Density, viscosity, refractive index and electrical conductivity of saturated solutions of the lithium hydroxide + ethanol + water system at 298.15 K, and thermodynamic description of the solid-liquid equilibrium. *Fluid Phase Equilib.* **2005**, *235*, 104–111.
(19) Zhu, Y.; Merkel, B. *The Dissolution and Solubility of Scorodite, $FeAsO_4 \cdot 2H_2O$. Evaluation and Simulation with PHREEQC2*; Wiss. Mitt. Inst. für Geologie, TU Bergakedemie Freiberg: Germany, 2001; Vol. 18.

Received for review February 3, 2009. Accepted June 19, 2009. Financial support from Conicyt (Fondecyt Project 1050869) and CICITEM is gratefully acknowledged.

JE900151S